Geophysical Research Letters

RESEARCH LETTER
10.1029/2020GL087486

Inverse Cascade Evidenced by Information Entropy of Passive Scalars in Submerged Canopy Flows

Khaled Ghannam[1], Davide Poggi[2], Elie Bou-Zeid[1], and Gabriel G. Katul[1,3,4]

[1]Department of Civil and Environmental Engineering, Princeton University, Princeton, NJ, USA, [2]Dipartimento di Ingegneria dell'Ambiente, del Territorio e delle Infrastrutture, Politecnico di Torino, Turin, Italy, [3]Nicholas School of the Environment, Duke University, Durham, NC, USA, [4]Department of Civil and Environmental Engineering, Duke University, Durham, NC, USA

Key Points:
- Canopy drag and coherent boundary layer eddies dictate distinct spectral regimes of passive scalar fluctuations within canopies
- Data from a flume experiment stipulate a deterministic nature of von Kármán vortices compared to high-entropy ejection-sweep cycle
- Entropy production in wakes is associated with "information" flow from small to large scales suggesting parallels to inverse energy cascades

Correspondence to:
K. Ghannam,
kghannam@princeton.edu

Citation:
Ghannam, K., Poggi, D., Bou-Zeid, E., & Katul, G. G. (2020). Inverse cascade evidenced by information entropy of passive scalars in submerged canopy flows. *Geophysical Research Letters*, *47*, e2020GL087486. https://doi.org/10.1029/2020GL087486

Received 11 FEB 2020
Accepted 21 APR 2020
Accepted article online 29 APR 2020

Abstract Turbulent mixing of scalars within canopies is investigated using a flume experiment with canopy-like rods of height h mounted to the channel bed. The data comprised a time sequence of high-resolution images of a dye recorded in a plane parallel to the bed at $z/h = 0.2$. Image processing shows that von Kármán wakes shed by canopy drag and downward turbulent transport from upper canopy layers impose distinct scaling regimes on the scalar spectrum. Measures from information theory are then used to explore the dominant directionality of the interaction between small and large scales underlying these two spectral regimes, showing that the arrival of sweeps from aloft establishes an inertial-range spectrum with forward "information" cascade. In contrast, wake growth with downstream distance leads to persistent upscale transfer (inverse cascade) of scalar variance, which hints at their nondiffusive character and the significance of the stem diameter as an active length scale in canopy turbulence.

Plain Language Summary Diagnosing the complex flow mechanisms that control mass transport and dispersion within forest canopies or vegetated streams is required in a plethora of applications spanning atmospheric and climate sciences, earth system modeling, ecology, and hydrology. Examples include pollen dispersal, residence time of volatile organic compounds, and aerosol deposition onto the forest floor. The work here uses data collected from a water channel experiment with rods mounted to the channel bottom representing a vegetated surface to explore how the eddying motion produced by canopy elements, and their disruption by larger eddies generated above the canopy, affects the transport and mixing of a dye (scalar) injected near the channel floor. The acquired data comprise a time sequence of planar images of the dye concentration that allow the investigation of how the small-sized eddies interact with large ones so as to influence the properties of the dye concentration in time. It is shown that as the flow impinges on stems, organized eddying structures called von Kármán streets are created. Using methods borrowed from information theory and applied at multiple spatial scales shows that these structures exhibit features that are counterintuitive to the way scalars typically disperse in flows without vegetation.

1. Introduction

The transport and mixing of scalar quantities (e.g., CO_2, water vapor, and aerosols) within vegetation canopies remain a challenging process to represent in modeling land-atmosphere interactions for weather and climate simulations (Patton et al., 2016), nutrient replenishment in vegetated streams (Nezu & Sanjou, 2008), and numerical simulations of geophysical flows (Calaf et al., 2011). Because the vertically extended drag canopies exert on an otherwise smooth/rough wall boundary layer flow, the turbulent transport process encodes a superposition of eddies emanating from distinct physical mechanisms and acting at different spatial scales. These vortical structures include attached eddies to some displaced height above the ground, shear instability (Kelvin-Helmholtz like) eddies near the canopy top for which the canopy height (h) serves as a characteristic length scale (Raupach et al., 1996), and wake turbulence in deeper layers of the canopy where the stem/trunk diameter (d_r) represents another characteristic length scale (e.g., Ghannam et al., 2018; Keylock et al., 2019; Poggi et al., 2004a). The former coherent eddies extract their turbulent kinetic energy (TKE) from the mean flow by strong shear at heights $z \sim h$ (Finnigan, 2000; Raupach et al., 1996),

inducing frequent downbursts (sweeping events) that ventilate the canopy volume at a period commensurate with h/u_* (Katul et al., 1998; Paw U et al., 1992; Raupach et al., 1996), where u_* is the friction velocity at the canopy top. In turn, TKE generation by form drag at scales $\sim d_r$ is associated with a wake-shedding mechanism that holds parallel to von Kármán vortices with a tendency to grow in size with downstream distance (Poggi et al., 2006). This complex eddy topology modulates the mixing properties of scalars within forest canopies or vegetated streams (Cava & Katul, 2008; Nepf & Ghisalberti, 2008), potentially invalidating common assumptions inherent to (i) first and higher-order closure models (Baldocchi, 1992; Poggi et al., 2004a; Shaw & Schumann, 1992) and (ii) spectral transfer theories that have canonically presumed a forward energy cascade (Danaila & Antonia, 2009; Leith, 1967). For instance, contaminant transport and tracer plume dispersion within canopies have been shown to depart from Fickian diffusion (Mossa et al., 2017; Murphy et al., 2007), requiring a diagnosis of the underlying interactions that shape the spatial variance of scalar fluctuations and its time evolution (i.e., dispersion coefficient). These interactions are also often unresolved in large eddy simulation (LES) of canopy turbulence (where vegetation is represented as a drag force), and hence, the formulation of subgrid-scale (SGS) models necessitates a meticulous treatment of wake-scale energy and possible upscale transfer effects (Shaw & Patton, 2003).

A number of field and laboratory experiments of canopy flows suggest that turbulence generated in the wake of plant elements short circuits the inertial subrange (ISR) of the energy cascade such that the high wavenumber ($k \gg d_r^{-1}$) regime of the scalar spectrum, similar to its velocity counterpart, exhibits steeper decay than the canonical $k^{-5/3}$ power law (e.g., Cava & Katul, 2008; Finnigan et al., 2009; Wilson, 1988). The conversion of mean kinetic energy to wake-scale energy by canopy drag is often cited as the cause of this short circuiting (i.e., bypassing the ISR) (Shaw, 1985), which in turn has motivated the treatment of wake turbulence as a rapidly dissipative (diffusive) process in SGS models of LES (Shaw & Patton, 2003). However, the validity of this framework remains difficult to establish or justify, in part because TKE production by vortex shedding is in competition with the periodic arrival of turbulent transport from the canopy top by sweeping events. This competition results in a short-circuited (rapidly decaying) scalar spectrum that is periodically interrupted as the ejection-sweep cycle reestablishes an ISR spectral scaling—an oscillatory behavior that has been depicted in flume experiments (Poggi et al., 2006, 2011). More importantly, the notion that wake turbulence accelerates the dissipation process inherently presumes a forward energy cascade, but experiments and theoretical arguments have identified strong structural parallels between von Kármán vortices and two-dimensional turbulence (Poggi et al., 2011), namely, that the spatial growth of these vortices concentrates the scalar variance (integral of the spectrum) in a narrow and low wavenumber range around the energy injection scale d_r. While this analogy is further motivated by the established result that velocity spectra exhibit a similar steep decay ($\sim k^{-3}$) in two-dimensional turbulence (Lesieur & Herring, 1985), the lack of an analogue to enstrophy (quadratic invariant of motion) in the scalar field prohibits the formalization of such an analogy.

To circumvent this issue, methods from information theory are used here to investigate the underlying mechanisms leading to distinct and time-dependent scaling of the spectra of scalar fluctuations within canopies (Poggi et al., 2004b). The working hypothesis rests on the existence of a unique entropy-producing mechanism when scalar mixing is controlled by canopy-induced wakes. This mechanism arises from small-scale to large-scale scalar variance flow reinforced by the growth of von Kármán vortices with downstream distance, rather than a prototypical vortex stretching and self-amplification (forward cascade) common to many types of locally homogeneous and isotropic turbulent flows (Carbone & Bragg, 2020). Toward this end, flume experiments are used in which scalar concentration fluctuations were sampled with laser-induced fluorescence (LIF) at high spatial and temporal resolution in the lower layers of a uniform canopy composed of rigid rods (section 2). After discussing the scalar concentration spectrum and distribution of information entropy across wavenumbers in section 3, the evolution of the scalar plume and time-lagged mutual information between the scales of turbulence are presented in section 4, and closing remarks in section 5.

2. Experiments and Methods

The data used here were collected in an open-channel experiment with canopy-like elements introduced as stainless steel vertical rods mounted to the bottom wall of the channel (Ghannam et al., 2015; Poggi & Katul, 2006; Poggi et al., 2004a). The experiment was carried out in a large rectangular constant head recirculating channel, 18 m long, 0.9 m wide, and 1 m deep with glass side walls to permit the passage of laser light.

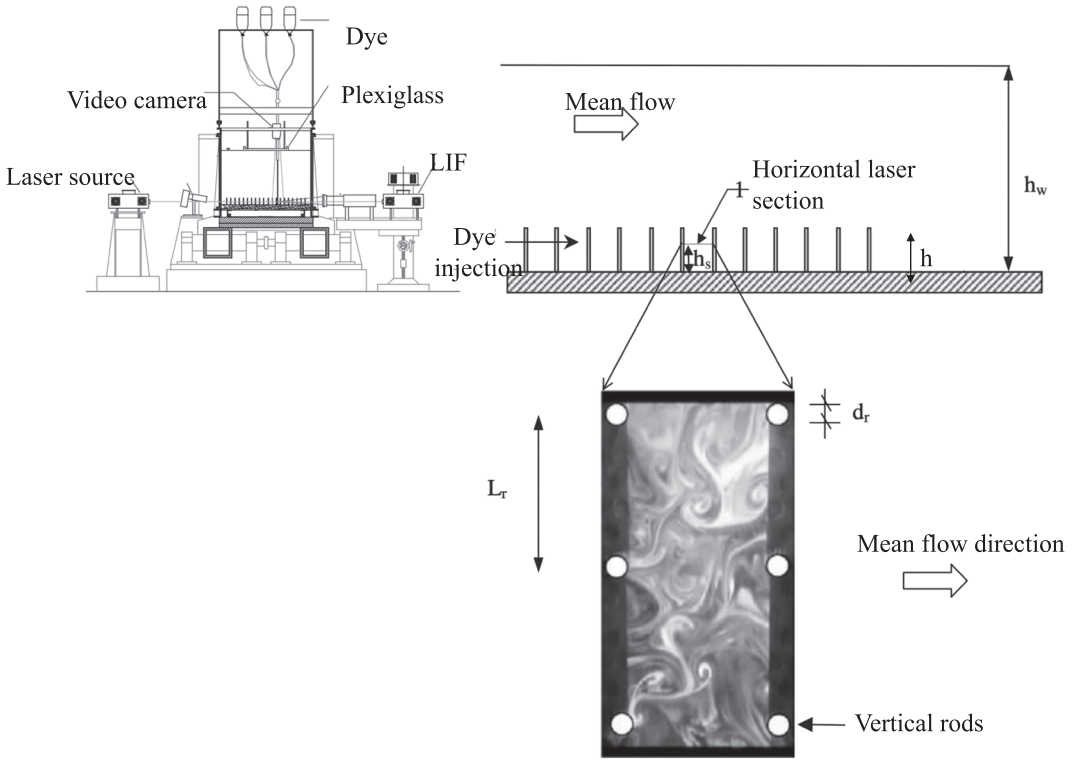

Figure 1. Schematic of the experimental setup. Top left: lateral section view showing the location of the LIF source and the video camera. Top right: longitudinal section view showing the dye release in relation to the model canopy. Bottom right: sample image at one instant in time of the 2-D relative scalar concentration field showing the generation of von Kármán streets. The rod diameter (d_r) and rod spacing (L_r) are also shown for reference. Adapted from Poggi and Katul (2006).

A schematic of the setup is shown in Figure 1. The height and diameter of the rod canopy are $h = 0.12$ m and $d_r = 4 \times 10^{-3}$ m, respectively, arrayed in a uniform square pattern at a density $n_p = 1,072$ rods·m^{-2} and situated in a test section 9-m downstream from the flume inlet. The local instantaneous dye concentration in a plane parallel to the channel bottom was measured using the LIF technique. The concentration measurements were conducted by (i) injecting Rhodamine 6G as a tracer, (ii) providing a horizontal light sheet between two lines of rods using a lens system, and (iii) recording a time sequence of images at high frequency (Figure 1). The light source was provided by a 300-mW continuous fixed wavelength ion-argon laser (Melles Griot mod.543-A-A03), and the images were recorded at a frequency of 30 Hz using a color charge-coupled device (CCD) video camera. These digital movies have a spatial resolution of 170×10^{-6} m and were collected at a height $z/h = 0.2$ (dye injection is at $z/h = 0.05$), where z is the vertical distance from the smooth channel bottom. The experiment was repeated three times resulting in three 72-s videos (2,148 images each) that were then used to compute instantaneous two-dimensional planar concentration. The results presented hereafter were similar across the three sequences. In addition, the rod spacing is $L_r = 30 \times 10^{-3}$ m ($7.5\, d_r$), and the friction velocity at the canopy top is $u_* = 0.045$ m·s^{-1}. The latter was estimated as $u_* = \sqrt{-\overline{u'w'}}$ using laser-Doppler anemometry measurements (Ghannam et al., 2015; Poggi et al., 2006). At room temperature, the molecular diffusivity of Rhodamine 6G in water is about $D = 4 \times 10^{-10}$ m^2·s^{-1}, whereas the molecular viscosity of water is $\nu = 1 \times 10^{-6}$ m^2·s^{-1}, that is, the molecular Schmidt number $Sc = \nu/D = 2500 \gg 1$, and the flow resides in the inertial-convective subrange (Leith, 1967; Lesieur & Herring, 1985). In this range, molecular diffusion is sensed at much smaller scales than viscous effects. In the absence of canopy elements, scalar spectra in the inertial-convective regime are presumed to be insensitive to variations of scalar fluctuations at large scales.

The instantaneous scalar concentration $\Theta(\mathbf{x}, t)$ obtained from LIF measurements is decomposed into a spatial mean (for each of the 2,148 images) and fluctuating parts, namely, $\Theta(\mathbf{x}, t) = \langle\Theta\rangle(t) + \Theta'(\mathbf{x}, t)$, where $\mathbf{x} \equiv (x, y)$ is a plane parallel to the channel bottom with x being the streamwise direction and y the lateral direction; t is time; $\langle\cdot\rangle$ is an instantaneous average over (x, y); and primes indicate turbulent fluctuations

around this spatial average at a given time t. The statistic $\langle\Theta\rangle(t)$ is not expected to be stationary (i.e., its statistics are unsteady); in fact, this transient behavior of eddy topology switching between wake turbulence and sweeping eddies within the canopy motivates the work here. Hence, time averaging is avoided. To compute spectra (or structure functions), information entropy, and other statistics, scalar concentration increments are defined as

$$\theta(\mathbf{x}, r, t) = \Theta\left(\mathbf{x} + r\mathbf{e}_\mathbf{r}, t\right) - \Theta(\mathbf{x}, t), \tag{1}$$

where e_r is the unit vector in the radial direction and $r = \sqrt{x^2 + y^2}$ is the radial separation distance juxtaposition to scale or eddy sizes in the planar direction. While θ depends on the position $\mathbf{x}$ (or origin of the coordinate system), its probability density function (pdf), $p_\theta(r, t)$, is considered to be a function of r and t only (i.e., the flow is locally homogeneous in the plane parallel to the ground). This simplifying assumption rests on selecting the origin of the coordinate system (x, y) as the center of the horizontal plane (image) and restricting the analysis to radial separation distances in the range $0 \leq r \leq 2d_r$. Hence, the scalewise analysis is confined to a region in the flow that is relatively far from the immediate vicinity of the canopy elements (rod spacing is $7.5d_r$) and where symmetry in flow statistics is likely to hold. We also note that the contribution of dispersive fluxes is negligibly small for this dense and uniform canopy ($n_p = 1,072$ rods·m^{-2}) (Poggi et al., 2004b). The pdf $p_\theta(r, t)$ represents an empirical distribution of the concentration increments for each separation distance r at time t, namely, that the second moment of p_θ (or variance of θ) at time t is the value of the second-order structure function $\langle\theta(r)^2\rangle$. With this configuration, the two-dimensional spectrum $\phi_\theta(k)$ at any time t integrates to the spatial variance, namely,

$$\langle\Theta'^2\rangle = \int_0^\infty \phi_\theta(k)\mathrm{d}k, \tag{2}$$

where $k = 1/r = (k_x^2 + k_y^2)^{1/2}$ is the resultant radial wavenumber and, as before, its inverse is a surrogate for eddy sizes in the planar direction. It is the genesis of the scaling regimes of this spectrum and hence the contribution of eddy scales to the scalar variance $\langle\Theta'^2\rangle(t)$ that is sought. The focus is on how von Kármán vortices (hereafter von Kármán flow) and downward sweeps associated with coherent eddies (hereafter sweeping flow) impact the scaling laws of $\phi_\theta(k)$ for the range $0 \leq r \leq 2d_r$.

The second-order structure function $\langle\theta^2\rangle(r, t)$ is an equivalent representation to $\phi_\theta(k, t)$ (cumulative contribution of scales r to $\langle\Theta'^2\rangle$) and is the second moment of $p_\theta(r, t)$. Hence, topological measures from information theory can be used to characterize the degree of organization and mutual information between eddies of size r that underlies the aforementioned scaling of the scalar spectrum. For instance, the Shannon (information) entropy associated with p_θ is

$$H_\theta(r, t) = -\sum_\theta p_\theta(r, t) \ln\left[p_\theta(r, t)\right], \tag{3}$$

where the sum is performed over all discrete empirical realizations of θ, giving then the entropy contained in a scale r (or wavenumber k) at time t. The quantity $H(r, t)$ is interpreted here as a measure of the degree of organization (predictability) of the concentration increments θ at the scale r (Wesson et al., 2003), with high entropy values indicating lack of organization (knowledge of scalar statistics at scale r provides no information about other scales). It must be emphasized that other interpretations of $H(r, t)$ exist (see, for instance, Ben-Naim, 2008) but the exercise here provides a means to contrast the distribution of H_θ and ϕ_θ across scales k, in turn revealing whether the steep spectral decay during von Kármán flow or the ISR scaling imposed by sweeping events arises from an organized process. To avoid potential sensitivity to the number of bins used in the evaluation of the empirical pdf to compute $H_\theta(r, t)$, we normalize H_θ by the entropy of a white noise process $H_\zeta(r, t)$ having the same number of bins as the scalar concentration fluctuations. The process $\zeta(r, t)$ is a Gaussian white noise generated empirically to have the same dimension (or size), mean, and variance of $\theta(r, t)$ for each analyzed image. Note that $\zeta(r, t)$ is devoid of any organization at all scales and has flat spectrum (or no autocorrelation), thereby ensuring that $H_\zeta(r, t)$ is maximum at all r. This bounds the ratio to $0 < H_\theta/H_\zeta < 1$ and provides a comparison between the entropy of θ and that of a white noise.

The nature of upscale spectral transfer associated with the spatial growth of stem wakes is further investigated by probing the direction of "information" cascade between scales. That is, the analysis seeks to address whether the cascade in scalar variance follows the canonical large-scale to small-scale trajectory (assumed in all spectral transfer theories for locally homogeneous and isotropic turbulence) or vice versa. For this

purpose, two sets of experiments are conducted with the time series of LIF images. The first starts with an initial concentration increment $\theta(r_0, t_0)$ with $r_0 \ll d_r$ (small scales) and defines a sequence of variables θ_d as the delayed/lagged concentration increments, that is, $\theta_d \equiv \theta(r_0 + \delta, t_0 + \tau)$, where δ and τ are positive spatial and temporal lags, respectively. The mutual information content, or relative entropy, between θ and θ_d is then defined by

$$\begin{aligned} I_{\theta,\theta_d} &= H_\theta + H_{\theta_d} - H_{\theta,\theta_d} \\ &= -\sum_{\theta,\theta_d} p_{\theta,\theta_d} \ln\left(\frac{p_{\theta,\theta_d}}{p_\theta \;\; p_{\theta_d}}\right), \end{aligned} \tag{4}$$

where $H_{\theta,\theta_d}(r,t)$ is the joint entropy associated with the joint distribution $p_{\theta,\theta_d}(r,t)$. The second line in equation (4) expresses relative entropy I_{θ,θ_d} as the Kullback-Leibler (KL) divergence, which vanishes if and only if $p_{\theta,\theta_d} = p_\theta \; p_{\theta_d}$ (i.e., when θ and θ_d are independent) and is positive otherwise. In this form, I_{θ,θ_d} can be interpreted as the expected value of the difference between the "surprise" of finding information about the large scales θ_d starting with small scales $\theta(r_0, t_0)$, that is, $\ln\left[p_{\theta,\theta_d}\right]$, and finding them to be independent, $\ln\left[p_\theta \; p_{\theta_d}\right]$. This concept is intricately related to internal entropy production due to the fact that θ and θ_d are not independent.

The second experiment starts with the initial condition $\theta(d_r, t_0)$ (i.e., large scales) with the same t_0 as the first experiment but constructs a reverse sequence of the first experiment; namely, the delayed concentration difference is now $\theta_d \equiv \theta(d_r - \delta, t_0 + \tau)$. It is important to observe that the latter sequence is the reverse of the first experiment in the scale r only. These two experiments, when conducted over time periods when the flow regime is dominated by canopy wakes or by the ejection-sweep cycle, serve the purpose of revealing whether entropy production (I_{θ,θ_d}) follows from small-scale to large-scale information flux (inverse cascade) or vice versa for each of these flow regimes. This analysis will be discussed further as part of the results (Figure 5) in section 4.

3. Spectra and Information Entropy

Figure 2a shows a time series of the spatial variance $\langle\Theta'^2\rangle(t)$ normalized by the corresponding instantaneous average $\langle\Theta\rangle(t)$ (i.e., squared coefficient of variation in space) for a time interval of $15h/u_*$. The ratio $\langle\Theta'^2\rangle/\langle\Theta\rangle^2$ can also be viewed as a measure of spatial turbulence intensity of the scalar, and we note that the time series of $\langle\Theta'^2\rangle$ itself shows a similar behavior. The analysis in Figure 2a reveals significant turbulence intensity ($20 < \langle\Theta'^2\rangle/\langle\Theta\rangle^2 < 90$) at all times, yet a quasiperiodic oscillatory behavior is evident with a period that roughly scales with h/u_*. The latter dynamical behavior of persistently large or small scalar variance not only is merely due to the inherent randomness of turbulence but also encodes a signature of the alternating nature of the dominant eddy topology. The large and small excursions in Figure 2a appear to be connected with whether the flow is modulated by von Kármán vortex shedding (large excursions) or coherent boundary layer eddies (small excursions). An example of this eddy topology is depicted in Figures 2b and 2c, showing instantaneous images of the flow during a sweeping event and during a wake-dominated regime, respectively. These images correspond to the instances marked by vertical dashed lines in Figure 2a, and a comprehensive inspection of all images showed a similar pattern: The arrival of downbursts from the canopy top disrupts the tendency of von Kármán vortices to establish a two-dimensional flow pattern, hence smearing out the effects of form drag on the scalar spectrum. This is noticeable in the 2D spectrum $\phi_\theta(k)$ for these two images in Figure 2d, showing a more extensive ISR ($k^{-5/3}$ scaling) associated with sweeping events and spanning approximately half a decade of scales $1 < kd_r < 5$. Conversely, $\phi_\theta(k)$ exhibits a steeper decay in the high wavenumber range as energy injection at $k_i \sim d_r$ reestablishes a wake dominated flow regime such that the scalar variance, albeit larger than its counterpart during sweeping events, builds up at scales commensurate with the stem diameter d_r (Figure 2d). The focus on the interplay between only downward turbulent transport (sweeps) and canopy drag assumes that the ejection component of the sweep-ejection cycle is a less efficient transport mechanism. It has been well established that sweeps dominate momentum transport inside canopies when compared to ejections (Poggi et al., 2004a). While Poggi et al. (2011) discussed the alternating scaling laws of $\phi_\theta(k)$ by investigating the spectral budget of the scalar conservation equation, here we refocus the attention on the statistical structure underlying these regimes.

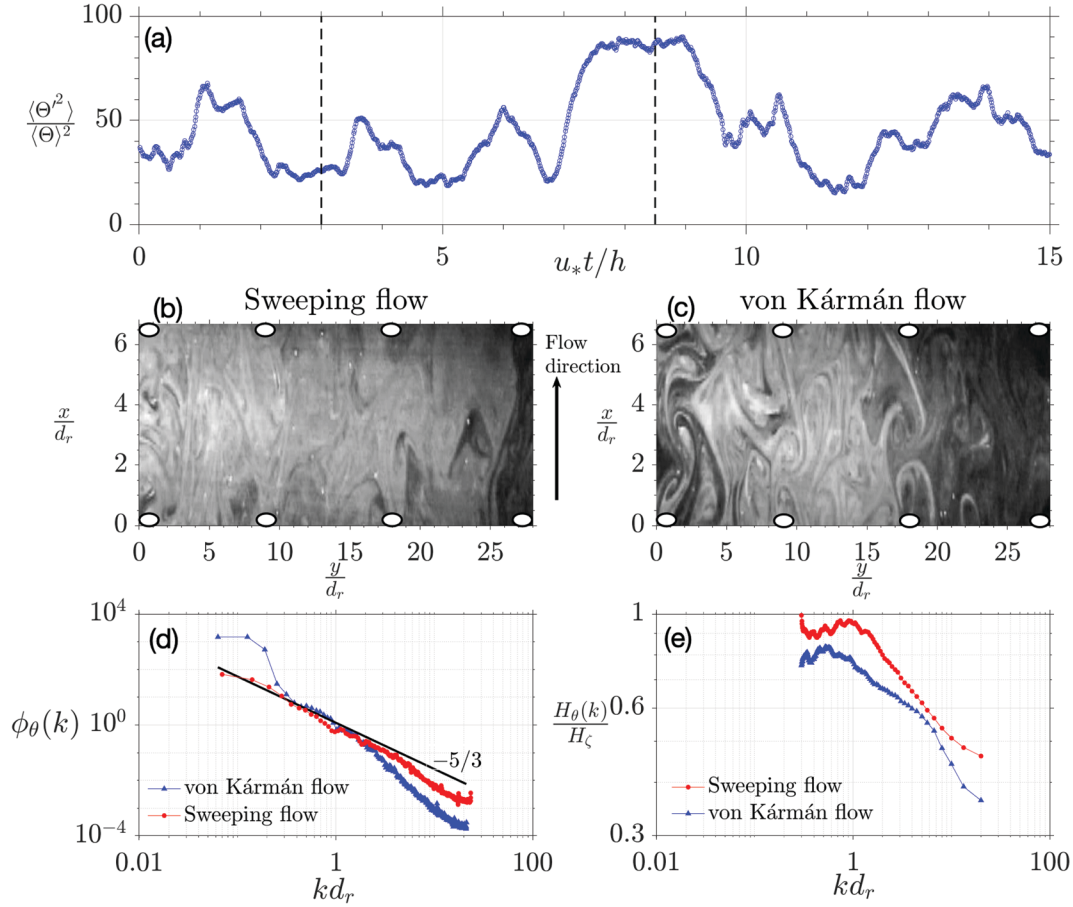

Figure 2. Flow characteristics in deep canopy layers ($z/h = 0.2$). (a) Time series of spatial scalar variance $\langle\Theta'^2\rangle$ normalized by its corresponding spatial mean as a measure of turbulence intensity. Time is normalized by h/u_* (periodicity of sweeping events). (b) and (c) correspond to two instantaneous images at times denoted by dashed vertical lines in (a). The lowest panels (d) and (e) show the spectra and information entropy (normalized by that of a white noise process H_ζ) for these two images.

Figure 2e shows the normalized information entropy (H_θ/H_ζ) (cf. equation 3) corresponding to the spectra in Figure 2d. For both flow regimes, the entropy of the concentration increments $\theta(r)$ increases with spatial scale and attains a constant (comparable to a white noise process) at scales larger than d_r; this flattening in H_θ at large scales ($kd_r < 1$) is an attribute of the Gaussian (and white noise) nature of $\theta(r > d_r)$. While this scale dependence of H_θ is not surprising since the variance of θ is itself an increasing function of r (cf. the structure function $\langle\theta^2(r)\rangle$), a peculiar feature in Figure 2e links the steep spectral decay associated with stem wakes (shown in Figure 2d) to a sharp decay in entropy at high wavenumbers, indicating that von Kármán vortices arise from a more organized quasideterministic process. On the other hand, the extensive ISR brought about by three-dimensional coherent eddies sweeping into the canopy appears to be driven by more random events with consistently less spatial organization (higher entropy) compared to wake turbulence at all scales (Figure 2e). This sharp contrast between the higher entropy of sweeping flow (ISR turbulence) and von Kármán streets hints at the self-organizing nature of the wake shedding mechanism as two-dimensional vortices tend to coalesce and grow in size before colliding with downstream canopy obstacles.

Figure 3 depicts the pdf p_θ at different scales r during these transient flow regimes. Note that the identification of periods (consecutive sequence of images) where the flow is dominated by wakes or sweeping events follows from an extensive examination of the scalar spectrum and entropy as discussed earlier and shown in Figures 1d and 2e. During transient periods of von Kármán flow (left panel in Figure 3), the variance of θ at small scales ($r \ll d_r$ shown in blue color) is significantly smaller than its counterpart during sweeping flow (right panel of Figure 3) and appears to be scale separated from larger scales ($r \sim d_r$). This separation

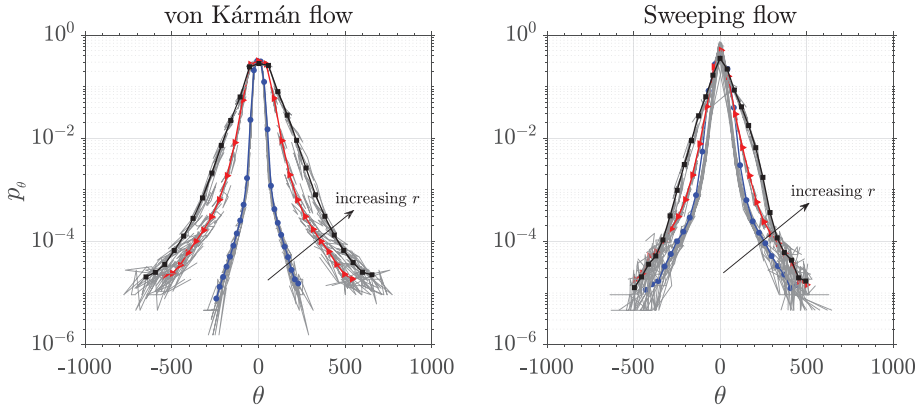

Figure 3. Probability density functions (pdf) of scalar concentration increments $\theta(r,t)$ during times of von Kármán flow (left panel) and sweeping events (right panel). (Color online) The gray solid lines are instantaneous realizations of p_θ at three eddy sizes: $r \ll d_r$, $r \sim d_r$, and $r > d_r$, with solid lines being their corresponding "ensemble" averages.

is additionally indicative of a build up of the variance at large scales ($r \sim d_r$) during wake-dominated periods (black line in Figure 3a) compared to a more evenly distributed scalewise contribution during sweeping events. To this end, and as we identified the distinguishing features imposed by stem wakes and coherent eddies on the scalar spectrum and scalewise entropy, we now turn our focus to the time evolution of the scalar plume and the interactions between scales r during these two transient periods.

4. Cascade Asymmetry and Entropy Production

Figure 4 shows a time transect of the longitudinal variance $\langle \Theta'^2 \rangle_x$ of the scalar plume for one time period h/u_* during von Kármán flow (upper panel) and sweeping flow (lower panel), where the subscript x indicates averaging over the streamwise direction. These representative periods (time transects) for each flow regime are identified from the time series in Figure 2a (as discussed earlier), corresponding to the time ranges $[8h/u_*, 9h/u_*]$ for the von Kármán flow and $[2h/u_*, 3h/u_*]$ for the sweeping flow in Figure 2a. Also, note that the vertical axis in Figure 4 is the lateral spread of the scalar plume (i.e., spread over y/d_r).

The longitudinal variance and its time evolution (dispersion coefficient) are necessary aspects for modeling contaminant transport and fate in natural and engineered systems, a field that has traditionally relied on Fickian diffusion approximation. In the aforementioned Fickian diffusion approximation, the central limit theorem leads to $\langle \Theta'^2 \rangle_x$ increasing linearly in t for large times (away from the source) with a dispersion coefficient that becomes constant (but see, e.g., Murphy et al., 2007). As shown earlier, the oscillatory nature of the scalar variance within canopies in Figure 2a allows further inquiry into the tendency of wake turbulence to prevent plume spread such that $\langle \Theta'^2 \rangle_x$ decreases with time and becomes more peaked (Figures 4a and 4b). Conversely, sweeping events restore canonical plume dispersion characteristics (Figures 4c and 4d).

Using the same time periods, namely, $[8h/u_*, 9h/u_*]$ for the von Kármán flow and $[2h/u_*, 3h/u_*]$ for the sweeping flow (Figure 2a), Figure 5 depicts the direction of entropy production (or time arrow) associated with the asymmetry in the "information" cascade during each of these flow regimes. The quantity shown on the y-axis is the relative entropy I_{θ,θ_d} calculated according to equation (4), either starting with $r_0 \ll d_r$ and hence θ_d being the concentration increment at larger scales $r = r_0 + \delta$ at later times $t = t_0 + \tau$ (defined as small-sclae to large-scale interactions) or vice versa for large to small scales (starting with $r_0 = d_r$ and θ_d being the concentration increment at smaller scales $r = d_r - \delta$ but still at later times $t = t_0 + \tau$). These two experiments conducted for each flow regime provide a means of tracking the direction of information cascade with time τ. Note that t_0 is chosen as the beginning of the analysis period for each flow regime, that is, $t_0 = 2h/u_*$ for sweeping flow and $t_0 = 8h/u_*$ for von Kármán flow. Figure 5a shows that vortex shedding by canopy elements restricts mutual information content to a small-scale to large-scale trajectory; that is, I_{θ,θ_d} increases with time τ, and internal entropy production is associated with information cascading from $\theta(r \ll d_r)$ to larger scales (inverse cascade). A similar analysis for the reverse sequence and for the same time period (von Kármán flow in Figure 5a) depicts virtually no entropy production following

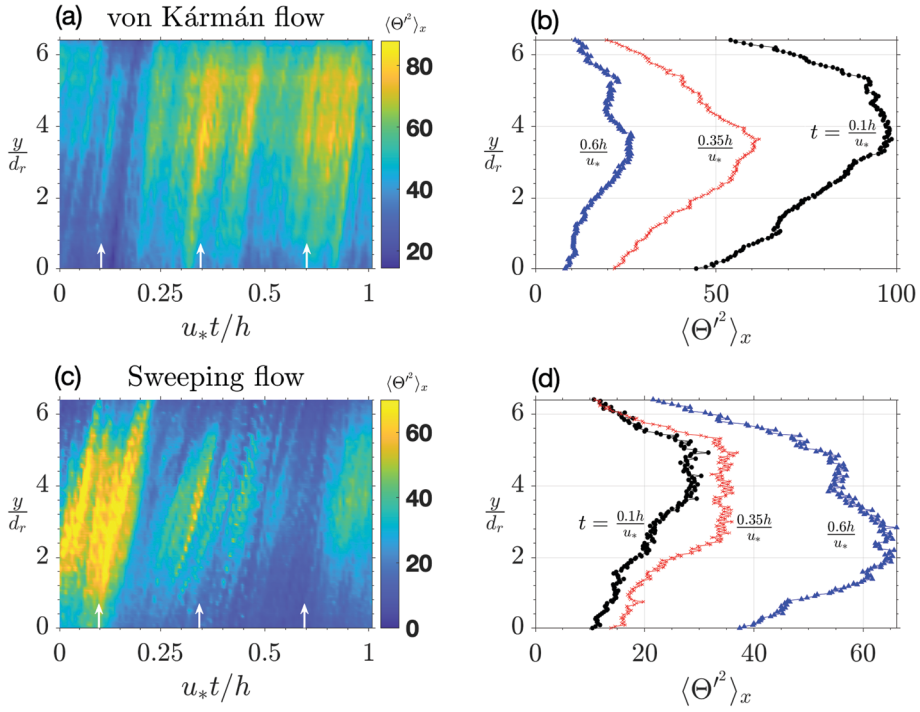

Figure 4. Time evolution of the longitudinal variance $\langle\Theta'^2\rangle_x$ of the scalar plume during wake-dominated flow regimes (upper panels a and b) and during sweeping flow (lower panels c and d). Panels (b) to (d) are three instantaneous realizations marked by small white arrows in (a) and (c), respectively.

a large-scale to small-scale trajectory. Conversely, the flow regime dominated by sweeps from the canopy top exhibits a canonical Richardson-like (large to small scale) information cascade (Figure 5b). Overall, the analysis here points to the likelihood that scalar fluctuations in the wakes of canopy elements are dominated by quasideterministic motion that resembles 2D turbulence. This resemblance is confined to periods with information/energy flow toward large scales, rather than to periods where the canonical forward cascade dominates.

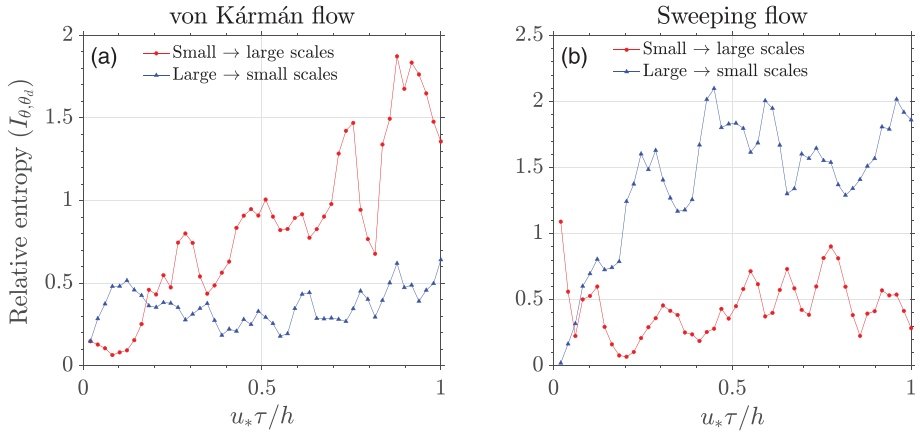

Figure 5. Direction of entropy-producing interactions during (a) von Kármán flow and (b) sweeping flow events. In (a), relative entropy between small eddies and larger eddies increases in time, while large → small scales remain essentially constant, suggesting an inverse cascade by canopy wakes. In (b), an inertial range turbulence restores a large → small scales cascade in entropy (see equation 4).

5. Concluding Remarks

The dynamics of passive scalar statistics within canopies were investigated using LIF measurements of dye concentration in a plane parallel to a flume bed with solid rods mimicking a uniform canopy configuration. It is shown that the steep decay in the two-dimensional spectrum of passive scalars within the confines of the canopy is a consequence of the tendency of stem wakes (von Kármán streets) to spatially grow in size with downstream distance, even though its behavior cannot be entirely explained by the theory of two-dimensional turbulence. Hence, these wakes truncate the high wavenumber spectral regime and concentrate the scalar variance at scales commensurate with the stem diameter d_r. This tendency is in sharp contrast to the ISR ($k^{-5/3}$) spectral scaling imposed by the periodic arrival of sweeping events from the canopy top. In reaching these conclusions, the dissimilarity in spectral scaling of instantaneous snapshots (images) of the flow was used to distinguish wake-dominated flow regimes and the arrival of downward sweeps from aloft. The corresponding scaling of information entropy was then used to illustrate that the aforementioned wake spectral scaling arises from organized and deterministic interactions between eddies. Analysis of the time and space-dependent mutual information content between turbulent scales disclosed a peculiar feature of scalar mixing by von Kármán vortices, namely, that internal entropy production is associated with increasing mutual information following a small-scale to large-scale information cascade, while canonical forward cascades remain dominant during the transient flow regime of sweeping events.

The broader implications of this work are threefold: (i) In Reynolds-averaged Navier-Stokes (RANS) models for scalar dispersion formulated in the deeper layers of tall canopies, there is no unique "master length scale." At minimum, two length scales must be used: h reflecting the Kelvin-Helmholtz vortices and their sweeping into the canopy and d_r reflecting the effects of von Kármán vortices. Should these effects be lumped into a single length scale, then a weighted length scale formulated based on the fraction of time the flow resides in sweeping motion and in wake-dominated regimes is required. This formulation may be possible due to the fact that scalar turbulence within the canopy appears to oscillate between these two classes of vortical motion. Clearly, such fraction must depend on vegetation density, but separate experiments using laser Doppler anemometry for momentum have indeed confirmed its feasibility (Poggi et al., 2004a). (ii) For spectral transfer models, the scalar transfer functions used, such as Leith's diffusion model or variants thereto (Hill, 1978; Leith, 1967; Rubinstein & Clark, 2013), must be assessed to accommodate backscatter effects. This topic is now gaining significant attention in physics and many geophysical applications where 3D-like turbulence and 2D-like turbulence coexist and impact energy content at many intermediate scales (Xia et al., 2011). Similar to RANS models, it may be possible to formulate two spectral transfer functions: one from large to small scales (analogous to Leith or Heisenberg or variants on them) and another from small to large scales (as with 2D turbulence) with relative weights based on the time fraction the flow resides in each spectral transfer mode. Developing a unified model that accounts for these findings is a research topic better kept for the future.

Acknowledgments
K. G. and G. K. acknowledge support from the U.S. National Science Foundation (NSF-AGS-1644382 and NSF-IOS-1754893). K. G. and E. B. Z. also acknowledge support from the Princeton Environmental Institute. All authors thank the anonymous reviewers for their constructive comments. The experimental data used in this work are archived at the DataSpace digital repository of Princeton University (Geophysical Fluid Dynamics Laboratory) with a persistent URL (http://arks.princeton.edu/ark:/88435/dsp01qj72pb044) and a DOI: https://doi.org/10.34770/7hyr-rf67.

References

Baldocchi, D. (1992). A Lagrangian random-walk model for simulating water vapor, CO_2 and sensible heat flux densities and scalar profiles over and within a soybean canopy. *Boundary-Layer Meteorology*, *61*(1-2), 113–144.

Ben-Naim, A. (2008). *Entropy demystified: The second law reduced to plain common sense*. Hackensack, N.J., USA: World Scientific.

Calaf, M., Parlange, M. B., & Meneveau, C. (2011). Large eddy simulation study of scalar transport in fully developed wind-turbine array boundary layers. *Physics of Fluids*, *23*(12), 126,603.

Carbone, M., & Bragg, A. D. (2020). Is vortex stretching the main cause of the turbulent energy cascade? *Journal of Fluid Mechanics*, *883*, p. R2. https://doi.org/10.1017/jfm.2019.923

Cava, D., & Katul, G. G. (2008). Spectral short-circuiting and wake production within the canopy trunk space of an alpine hardwood forest. *Boundary-Layer Meteorology*, *126*(3), 415–431.

Danaila, L., & Antonia, R. A. (2009). Spectrum of a passive scalar in moderate Reynolds number homogeneous isotropic turbulence. *Physics of Fluids*, *21*(11), 111702.

Finnigan, J. J. (2000). Turbulence in plant canopies. *Annual Review of Fluid Mechanics*, *32*(1), 519–571.

Finnigan, J. J., Shaw, R. H., & Patton, E. G. (2009). Turbulence structure above a vegetation canopy. *Journal of Fluid Mechanics*, *637*, 387–424.

Ghannam, K., Katul, G. G., Bou-Zeid, E., Gerken, T., & Chamecki, M. (2018). Scaling and similarity of the anisotropic coherent eddies in near-surface atmospheric turbulence. *Journal of the Atmospheric Sciences*, *75*(3), 943–964.

Ghannam, K., Poggi, D., Porporato, A., & Katul, G. G. (2015). The spatio-temporal statistical structure and ergodic behaviour of scalar turbulence within a rod canopy. *Boundary-Layer Meteorology*, *157*(3), 447–460.

Hill, R. J. (1978). Models of the scalar spectrum for turbulent advection. *Journal of Fluid Mechanics*, *88*(3), 541–562.

Katul, G. G., Geron, C. D., Hsieh, C.-I., Vidakovic, B., & Guenther, A. B. (1998). Active turbulence and scalar transport near the forest-atmosphere interface. *Journal of Applied Meteorology*, *37*(12), 1533–1546.

Keylock, C. J., Ghisalberti, M., Katul, G. G., & Nepf, H. M. (2019). A joint velocity-intermittency analysis reveals similarity in the vertical structure of atmospheric and hydrospheric canopy turbulence. *Environmental Fluid Mechanics*, *20*, 1–25.

Leith, C. E. (1967). Diffusion approximation to inertial energy transfer in isotropic turbulence. *The Physics of Fluids*, *10*(7), 1409–1416.

Lesieur, M., & Herring, J. (1985). Diffusion of a passive scalar in two-dimensional turbulence. *Journal of Fluid Mechanics*, *161*, 77–95.

Mossa, M., Meftah, M. B., De Serio, F., & Nepf, H. M. (2017). How vegetation in flows modifies the turbulent mixing and spreading of jets. *Scientific Reports*, *7*(1), 6587.

Murphy, E., Ghisalberti, M., & Nepf, H. (2007). Model and laboratory study of dispersion in flows with submerged vegetation. *Water Resources Research*, *43*, W05438. https://doi.org/10.1029/2006WR005229

Nepf, H., & Ghisalberti, M. (2008). Flow and transport in channels with submerged vegetation. *Acta Geophysica*, *56*(3), 753–777.

Nezu, I., & Sanjou, M. (2008). Turbulence structure and coherent motion in vegetated canopy open-channel flows. *Journal of Hydro-Environment Research*, *2*(2), 62–90.

Patton, E. G., Sullivan, P. P., Shaw, R. H., Finnigan, J. J., & Weil, J. C. (2016). Atmospheric stability influences on coupled boundary layer and canopy turbulence. *Journal of the Atmospheric Sciences*, *73*(4), 1621–1647.

Paw U, K. T., Brunet, Y., Collineau, S., Shaw, R. H., Maitani, T., Qiu, J., & Hipps, L. (1992). On coherent structures in turbulence above and within agricultural plant canopies. *Agricultural and Forest Meteorology*, *61*, 55–68.

Poggi, D., & Katul, G. (2006). Two-dimensional scalar spectra in the deeper layers of a dense and uniform model canopy. *Boundary-Layer Meteorology*, *121*(2), 267–281.

Poggi, D., Katul, G. G., & Albertson, J. D. (2004a). Momentum transfer and turbulent kinetic energy budgets within a dense model canopy. *Boundary-Layer Meteorology*, *111*(3), 589–614.

Poggi, D., Katul, G. G., & Albertson, J. D. (2004b). A note on the contribution of dispersive fluxes to momentum transfer within canopies. *Boundary-Layer Meteorology*, *111*(3), 615–621.

Poggi, D., Katul, G., & Albertson, J. (2006). Scalar dispersion within a model canopy: Measurements and three-dimensional Lagrangian models. *Advances in Water Resources*, *29*(2), 326–335.

Poggi, D., Katul, G. G., & Vidakovic, B. (2011). The role of wake production on the scaling laws of scalar concentration fluctuation spectra inside dense canopies. *Boundary-Layer Meteorology*, *139*(1), 83–95.

Poggi, D., Porporato, A., Ridolfi, L., Albertson, J. D., & Katul, G. G. (2004a). The effect of vegetation density on canopy sub-layer turbulence. *Boundary-Layer Meteorology*, *111*(3), 565–587.

Poggi, D., Porporato, A., Ridolfi, L., Albertson, J. D., & Katul, G. G. (2004b). Interaction between large and small scales in the canopy sublayer. *Geophysical Research Letters*, *31*, L05102. https://doi.org/10.1029/2003GL018611

Raupach, M. R., Finnigan, J. J., & Brunet, Y. (1996). Coherent eddies and turbulence in vegetation canopies: The mixing-layer analogy. *Boundary-Layer Meteorology*, *78*, 351–382.

Rubinstein, R., & Clark, T. T. (2013). Reassessment of the classical closures for scalar turbulence. *Journal of Turbulence*, *14*(2), 71–98.

Shaw, R. H. (1985). The dissipation of turbulence in plant canopies. In *7th Symp. American Meteorol. Society on Turbulence and Diffusion, 1985. 11*. Boulder, Colorado, USA.

Shaw, R. H., & Patton, E. G. (2003). Canopy element influences on resolved- and subgrid-scale energy within a large-eddy simulation. *Agricultural and Forest Meteorology*, *115*(1-2), 5–17.

Shaw, R. H., & Schumann, U. (1992). Large-eddy simulation of turbulent flow above and within a forest. *Boundary-Layer Meteorology*, *61*(1-2), 47–64.

Wesson, K. H., Katul, G. G., & Siqueira, M. (2003). Quantifying organization of atmospheric turbulent eddy motion using nonlinear time series analysis. *Boundary-Layer Meteorology*, *106*(3), 507–525.

Wilson, J. D. (1988). A second-order closure model for flow through vegetation. *Boundary-Layer Meteorology*, *42*(4), 371–392.

Xia, H., Byrne, D., Falkovich, G., & Shats, M. (2011). Upscale energy transfer in thick turbulent fluid layers. *Nature Physics*, *7*(4), 321–324.